Dicluster stopping in a degenerate electron gas

Hrachya B. Nersisyan[1] and Amal K. Das[2]
[1]*Theoretical Physics Division, Institute of Radiophysics and Electronics, Ashtarak-2, 378410, Armenia*
[2]*Department of Physics, Dalhousie University, Halifax, Nova Scotia, Canada B3H 3J5*
(Received 19 April 2000)

In this paper we report on our theoretical studies of various aspects of the correlated stopping power of two pointlike ions (a dicluster) moving in close but variable vicinity of each other in some metallic target materials, the latter being modeled by a degenerate electron gas with appropriate densities. Within the linear-response theory we have made a comprehensive investigation of correlated stopping power, vicinage function and related quantities for a diproton cluster in two metallic targets, aluminum and copper, and present detailed and comparative results for three approximations to the electron gas dielectric function, namely, the plasmon-pole approximation without and with dispersion as well as with the random-phase approximation. The results are also compared, wherever applicable, with those for an individual projectile.

PACS number(s): 52.40.Mj, 34.50.Bw, 61.85.+p, 71.45.Gm

I. INTRODUCTION

The stopping of energetic charged particles in a target material is a problem of long-standing theoretical and experimental interest. Early pioneering theoretical work by Bohr, who had a lifelong interest in this problem, was followed by Bethe and others. There is by now an extensive literature on this topic. We refer the reader to two recent review articles [1,2]. The problem in its generality is rather complex. However simplified theoretical models have been applied with considerable success in explaining experimental data. Assuming a weak coupling between the energetic particle and a target material, especially a metal which is usually approximated by a degenerate electron gas, a detailed theoretical model has emerged through the works of Bohm, Pines, Lindhard, Ritchie, and other authors [3–5].

A comprehensive treatment of the quantities related to inelastic particle-solid and particle-plasma interactions, e.g., scattering rates and differential and total mean-free-paths and energy losses, can be formulated in terms of the dielectric-response function obtained from the electron-gas model. The results have important applications in astrophysics [6,7] and radiation and solid-state physics [8–11], and more recently, in studies of energy deposition by ion beams in plasma fusion targets [12–16].

One can think of several situations in which the projectile beam ions may be closely spaced so that their stopping is influenced by their mutual interactions [14,15] and thus differs from the stopping of charged particles whose dynamics are independent of each other. This can happen, for example, in the case of very high-density beams, or more realistically, when cluster ions are to be used instead of standard ion beams [16].

The stopping of uncorrelated or independent charged particles in a degenerate electron gas (DEG) has been extensively studied in the literature (see, for example, Refs. [3–9,13], and other references therein). These studies have been done mostly within the linear-response formalism and for the projectile velocity V comparable or greater than v_F, the electron Fermi velocity.

The objective of this paper is to make a study of the stopping power (SP) of correlated charged particles in a DEG. The simplest and yet physically relevant case is the SP of an ion pair (a dicluster). We report on a comprehensive investigation, which is mostly numerical, of various aspects of a dicluster stopping in a DEG. Previous theoretical works have considered this problem within the linear-response theory [9–11] and in a simple plasmon-pole approximation. In our paper, again in the linear-response formalism, we have used both the plasmon-pole approximation (PPA) as well as the full Lindhard expression for the random-phase approximation (RPA) in the DEG dielectric function. As in earlier studies we consider a diproton cluster as a projectile and compare our theoretical results with those of Basbas and Ritchie [10] who used PPA and with those obtained in RPA. Whenever applicable, the results are also compared with those for an independent projectile (e.g., those due to Yakolev and Kotel'nikov [7]). To our knowledge, no RPA results for a diproton cluster SP and related aspects have previously been reported in the literature.

II. STOPPING POWER

Let us consider an external charge with distribution $\rho_{\rm ext}(\mathbf{r},t)=Q_{\rm ext}(\mathbf{r}-\mathbf{V}t)$ moving with velocity $\mathbf{V}$ in a medium characterized by the longitudinal dielectric function $\varepsilon(k,\omega)$. Within the linear-response theory and in the Born approximation the scalar electric potential $\varphi(\mathbf{r},t)$ due to this external charge screened by the medium is given by [1]

$$\varphi(\mathbf{r},t)=4\pi\int d\mathbf{k}\,Q_{\rm ext}(\mathbf{k})\,\frac{\exp[i\mathbf{k}\cdot(\mathbf{r}-\mathbf{V}t)]}{k^2\varepsilon(k,\mathbf{k}\cdot\mathbf{V})}, \qquad (1)$$

where $Q_{\rm ext}(\mathbf{k})$ is the Fourier transform of function $Q_{\rm ext}(\mathbf{r})$.

The stopping power, which is the energy loss of the external charge regarded as a projectile, per unit path length in the medium regarded as a target material, can be calculated from the force acting on the charge. The latter is related to the induced electric field $\mathbf{E}_{\rm ind}$ in the medium. For a three-dimensional medium we have, for the SP,

$$S \equiv -\int d\mathbf{r}\; Q_{\rm ext}(\mathbf{r}-\mathbf{V}t)\cdot\frac{\mathbf{V}}{V}\mathbf{E}_{\rm ind}(\mathbf{r},t)$$

$$=\frac{2(2\pi)^4}{V}\int d\mathbf{k}|Q_{\rm ext}(\mathbf{k})|^2\frac{\mathbf{k}\cdot\mathbf{V}}{k^2}{\rm Im}\frac{-1}{\varepsilon(k,\mathbf{k}\cdot\mathbf{V})}. \qquad (2)$$

Equation (2) is applicable to any external charge distribution. We shall apply it to a cluster of two pointlike ions having charges Z_1e and Z_2e separated by a variable distance $\mathbf{R}$. For this dicluster

$$|Q_{\rm ext}(\mathbf{k})|^2=\frac{e^2}{(2\pi)^6}[Z_1^2+Z_2^2+2Z_1Z_2\cos(\mathbf{k}\cdot\mathbf{R})]. \qquad (3)$$

Then the stopping power of a dicluster may be written as

$$S=(Z_1^2+Z_2^2)S_{\rm ind}(V)+2Z_1Z_2S_{\rm corr}(\mathbf{R},V), \qquad (4)$$

where $S_{\rm ind}(V)$ and $S_{\rm corr}(\mathbf{R},V)$ stand for individual and correlated SP, respectively. From Eqs. (2) and (3),

$$S_{\rm ind}(V)=\frac{2e^2}{\pi V^2}\int_0^\infty\frac{dk}{k}\int_0^{kV}{\rm Im}\frac{-1}{\varepsilon(k,\omega)}\,\omega\,d\omega, \qquad (5)$$

$$S_{\rm corr}(\mathbf{R},V)=\frac{2e^2}{\pi V^2}\int_0^\infty\frac{dk}{k}\int_0^{kV}{\rm Im}\frac{-1}{\varepsilon(k,\omega)}\,\omega\,d\omega$$

$$\times\cos\left(\frac{\omega}{V}R\cos\vartheta\right)J_0\left(R\sin\vartheta\sqrt{k^2-\frac{\omega^2}{V^2}}\right). \qquad (6)$$

$J_0(x)$ is the Bessel function of the first kind and zero order and ϑ is the angle between the interionic separation vector $\mathbf{R}$ and the velocity vector $\mathbf{V}$. Equations (5) and (6) can also be obtained from the linearized Vlasov-Poisson equations for a two-ion projectile system, as has been done by Avanzo *et al.* [14]. In their study the target material is a dense classical electron gas.

We note that there are two contributions to the SP of a two-ion cluster. The first one, given by the first term in Eq. (4), is the uncorrelated particle contribution and represents the energy loss of the individual projectiles due to their coupling with the target electron gas. The second contribution, the second term in Eq. (4), arises due to a correlated motion of the two ions through a resonant interaction with the excitations of the electron gas. Both terms are responsible for an irreversible energy transfer from the two-ion projectile system to the target electron gas.

In many experimental situations, clusters are formed with random orientations of $\mathbf{R}$. A correlated stopping power appropriate to this situation may be obtained by carrying out a spherical average over $\mathbf{R}$ of the $S_{\rm corr}(\mathbf{R},V)$ in Eq. (4). We find

$$\overline{S}_{\rm corr}(R,V)=\frac{2e^2}{\pi RV^2}\int_0^\infty\frac{dk}{k^2}\sin(kR)\int_0^{kV}{\rm Im}\frac{-1}{\varepsilon(k,\omega)}\,\omega\,d\omega. \qquad (7)$$

One may consider an interference or vicinage function, which is a measure of the separation of single-particle contribution from its correlated counterpart, to the stopping power. This function is defined as [10,14,15]

$$\Gamma(\mathbf{R},V)=\frac{S_{\rm corr}(\mathbf{R},V)}{S_{\rm ind}(V)}. \qquad (8)$$

Equation (4) can then be put in the form

$$S=(Z_1^2+Z_2^2)S_{\rm ind}(V)\left[1+\frac{2Z_1Z_2}{Z_1^2+Z_2^2}\Gamma(\mathbf{R},V)\right]. \qquad (9)$$

$\Gamma(\mathbf{R},V)$ describes the strength of correlation effects with respect to an uncorrelated situation. The vicinage function becomes equal to unity as $R\to0$ when the two ions coalesce into a single entity, and goes to zero as $R\to\infty$ when the two ions are totally uncorrelated.

III. THEORETICAL CALCULATIONS OF SP

The key ingredient in the calculation of stopping power, as outlined in Sec. II, is the linear-response function $\varepsilon(k,\omega)$ of the target material. The latter is modeled in most cases by a dense electron gas neutralized by a positive background—the so-called jellium model. The effect of the lattice is not included except perhaps through an effective mass of the electrons. This is a reasonable model for target materials like Cu and Al. $\varepsilon(k,\omega)$ for a dense, and hence a degenerate electron gas, has been calculated in various approximations in the literature. Two of them are: (1) PPA and (2) RPA. Actually the plasmon-pole approximation is a simplification of the RPA response function. We shall consider SP in these two approximations.

A. SP in PPA without plasmon dispersion

Here we consider the simplest model of the dielectric function of a jellium. In Ref. [10] (see also the Ref. [15]) a plasmon-pole approximation to $\varepsilon(k,\omega)$ for an electron gas was used for calculation of dicluster SP. In order to get easily obtainable analytical results, Basbas and Ritchie [10] employ a simplified form that exhibits collective and single-particle effects

$${\rm Im}\frac{-1}{\varepsilon(k,\omega)}=\frac{\pi\omega_p^2}{2\omega}\left[H(k_c-k)\,\delta(\omega-\omega_p)\right.$$

$$\left.+H(k-k_c)\,\delta\left(\omega-\frac{\hbar k^2}{2m}\right)\right], \qquad (10)$$

where $H(x)$ is the Heaviside unit-step function, $\hbar\omega_p$ is the plasma energy of the electron gas, and the choice $k_c=(2m\omega_p/\hbar)^{1/2}$ allows the two δ functions in Eq. (10) to coincide at $k=k_c$ in the k-ω plane.

The first term in Eq. (10) describes the response due to nondispersive plasmon excitation in the region $k<k_c$, while the second term describes free-electron recoil in the range $k>k_c$ (single-particle excitations). This approximate function satisfies the sum rule

$$\int_0^\infty \mathrm{Im}\frac{-1}{\varepsilon(k,\omega)}\,\omega\,d\omega=\frac{\pi\omega_p^2}{2} \tag{11}$$

for all values of k.

In this approximation, if $V>(\hbar\omega_p/2m)^{1/2}\equiv V_p$,

$$S_{\mathrm{ind}}(\lambda)=\frac{e^2\omega_p^2}{V^2}\ln\left(\frac{2mV^2}{\hbar\omega_p}\right)=\frac{\Sigma_0}{\pi\chi^2\lambda^2}\ln\left(\frac{\lambda^2\sqrt{3}}{\chi}\right), \tag{12}$$

where $\lambda=V/v_F$, $\chi^2=1/\pi k_F a_0=(4/9\pi^4)^{1/3}r_s$; $r_s=(3/4\pi n_0 a_0^3)^{1/3}$, n_0 is the electron gas density, and $a_0=0.53\times10^{-8}$cm is the Bohr radius. k_F is the Fermi wave number of the target electrons and $\Sigma_0=2.18$ GeV/cm. In our calculations χ (or r_s) serves as a measure of electron density. The result in Eq. (12) agrees exactly with the Bethe SP formula, except that the plasmon energy of the electron gas $\hbar\omega_p$ appears instead of the usual mean atomic excitation energy. Equation (12) represents the contribution of valence/conduction electrons in a solid to the stopping of an ion.

Using Eq. (10) in Eq. (6), in the high-velocity limit $V>V_p$ (or $\lambda^2>\chi/\sqrt{3}\equiv\lambda_0^2$) one finds

$$\begin{aligned}S_{\mathrm{corr}}(R,\vartheta,\lambda)=\frac{\Sigma_0}{\pi\chi^2\lambda^2}\Bigg\{&\cos\left(\frac{2\chi}{\lambda\sqrt{3}}k_FR\cos\vartheta\right)\\&\times\int_1^{\lambda/\lambda_0}\frac{dx}{x}J_0\left(\frac{2\chi}{\lambda\sqrt{3}}k_FR\sin\vartheta\sqrt{x^2-1}\right)\\&+\int_{2\lambda_0}^{2\lambda}\frac{dx}{x}\cos\left(\frac{x^2}{2\lambda}k_FR\cos\vartheta\right)\\&\times J_0\left(xk_FR\sin\vartheta\sqrt{1-\frac{x^2}{4\lambda^2}}\right)\Bigg\}.\end{aligned} \tag{13}$$

If one ion trails directly behind the other ($\vartheta=0$) from Eq. (13) we find

$$\begin{aligned}S_{\mathrm{corr}}(R,0,\lambda)=\frac{\Sigma_0}{2\pi\chi^2\lambda^2}\Bigg\{&\cos\left(\frac{2\chi}{\lambda\sqrt{3}}k_FR\right)\ln\left(\frac{\lambda^2\sqrt{3}}{\chi}\right)\\&+\mathrm{ci}(2\lambda k_FR)-\mathrm{ci}\left(\frac{2\chi}{\lambda\sqrt{3}}k_FR\right)\Bigg\},\end{aligned} \tag{14}$$

where $\mathrm{ci}(z)$ is the integral cosine function

$$\mathrm{ci}(z)=-\int_z^\infty dx\frac{\cos x}{x}. \tag{15}$$

One sees a characteristic oscillatory behavior for large interionic distance R. As discussed in Ref. [16], fluctuations in the stopping power of a medium for a cluster as separation increases are due to electron-density variation in the wake of the leading ion. The wavelength of these fluctuations is $\sim 2\pi V/\omega_p$ for high-velocity projectiles.

In the case of randomly oriented clusters from Eq. (7) we find

$$\overline{S}_{\mathrm{corr}}(R,\lambda)=\frac{\Sigma_0}{\pi\chi^2\lambda^2}\left[\mathrm{si}_2\left(\frac{2\chi}{\lambda\sqrt{3}}(k_FR)\right)-\mathrm{si}_2[2\lambda(k_FR)]\right], \tag{16}$$

where

$$\mathrm{si}_2(z)=\int_z^\infty dx\frac{\sin x}{x^2}=\frac{\sin(z)}{z}-\mathrm{ci}(z). \tag{17}$$

B. SP in PPA with plasmon dispersion

Plasmons without dispersion are an idealization. In real systems plasmons are expected to undergo a dispersion leading to a $\omega(k)$. The actual dispersion (in RPA) can be obtained from the linear-response function (see Sec. III C). Here we shall utilize a dispersion that is valid for small and intermediate values of the wave vector $\mathbf{k}$. Consequently we write

$$\mathrm{Im}\frac{-1}{\varepsilon(k,\omega)}=\frac{\pi\omega_p^2}{2\omega}\delta[\omega-\Omega(k)], \tag{18}$$

where the dispersion is given by

$$\Omega^2(k)=\omega_p^2+\frac{3}{5}k^2v_F^2+\frac{\hbar^2k^4}{4m^2}. \tag{19}$$

In this approximation when

$$V>\left(\frac{3}{5}v_F^2+\frac{\hbar\omega_p}{m}\right)^{1/2}\equiv V_0 \tag{20}$$

we have, for individual and correlated SP,

$$S_{\mathrm{ind}}(\lambda)=\frac{\Sigma_0}{\pi\chi^2\lambda^2}\ln\frac{\lambda^2-3/5+\sqrt{(\lambda^2-3/5)^2-4\chi^2/3}}{2\chi/\sqrt{3}}, \tag{21}$$

$$\begin{aligned}S_{\mathrm{corr}}(R,\vartheta,\lambda)=\frac{\Sigma_0}{\pi\chi^2\lambda^2}&\int_{x_-(\lambda)}^{x_+(\lambda)}\frac{dx}{x}\\&\times\cos\left(\frac{\phi_1(x)}{2\lambda}k_FR\cos\vartheta\right)\\&\times J_0\left(\frac{\phi_2(x)}{2\lambda}k_FR\sin\vartheta\right).\end{aligned} \tag{22}$$

Here k_F is the Fermi wave number, and

$$\phi_1(x)=\sqrt{x^4+\frac{12}{5}x^2+16\chi^2/3}, \tag{23}$$

$$\phi_2(x)=\sqrt{4\left(\lambda^2-\frac{3}{5}\right)x^2-(x^4+16\chi^2/3)}, \tag{24}$$

$$x_\pm(\lambda)=\sqrt{2\left[\lambda^2-\frac{3}{5}\pm\sqrt{\left(\lambda^2-\frac{3}{5}\right)^2-\frac{4\chi^2}{3}}\right]}. \tag{25}$$

In the case of randomly oriented clusters we find

$$\overline{S}_{\rm corr}(R,\lambda)=\frac{\Sigma_0}{\pi\chi^2\lambda^2}\{{\rm si}_2[k_FRx_-(\lambda)]-{\rm si}_2[k_FRx_+(\lambda)]\}. \tag{26}$$

C. Stopping power in RPA

Now we will derive the analytical expressions for the SP of a dicluster in a fully degenerate ($T=0$) electron gas. For this purpose we use the exact RPA dielectric response function obtained by Lindhard [4]

$$\varepsilon(z,u)=1+\frac{\chi^2}{z^2}[f_1(z,u)+if_2(z,u)], \tag{27}$$

where

$$f_1(z,u)=\frac{1}{2}-\frac{1}{8z}(U_+^2-1)\ln\left|\frac{U_++1}{U_+-1}\right| + \frac{1}{8z}(U_-^2-1)\ln\left|\frac{U_-+1}{U_--1}\right|, \tag{28}$$

$$f_2(z,u)=\begin{cases}\dfrac{\pi}{8z}[1-(u-z)^2];\ \ |u-1|\leqslant z\leqslant u+1\\ 0;\ \ 0\leqslant z\leqslant u-1,\\ 0;\ \ z\geqslant u+1,\\ \dfrac{1}{2}\pi u;\ \ 0\leqslant z\leqslant 1-u\end{cases}. \tag{29}$$

Here, as in Refs. [6], [7], [13], and [15], we have introduced the following notations: $z=k/2k_F$, $u=\omega/kv_F$, and $U_\pm=u\pm z$. With these notations Eqs. (5), (6), and (7) read

$$S_{\rm ind}(\lambda)=\frac{6\Sigma_0}{\pi^2\chi^2\lambda^2}\int_0^\infty z^3dz\int_0^\lambda\frac{f_2(z,u)u\,du}{[z^2+\chi^2f_1(z,u)]^2+\chi^4f_2^2(z,u)}, \tag{30}$$

$$S_{\rm corr}(\lambda,R,\vartheta)=\frac{6\Sigma_0}{\pi^2\chi^2\lambda^2}\int_0^\infty z^3dz \times\int_0^\lambda\frac{f_2(z,u)u\,du}{[z^2+\chi^2f_1(z,u)]^2+\chi^4f_2^2(z,u)} \times\cos\left(2\frac{zu}{\lambda}k_FR\cos\vartheta\right) \times J_0\left(2zk_FR\sin\vartheta\sqrt{1-\frac{u^2}{\lambda^2}}\right), \tag{31}$$

$$\overline{S}_{\rm corr}(R,\lambda)=\frac{3\Sigma_0}{\pi\lambda^2}\frac{a_0}{R}\int_0^\infty\sin(2k_FRz)z^2dz \times\int_0^\lambda\frac{f_2(z,u)u\,du}{[z^2+\chi^2f_1(z,u)]^2+\chi^4f_2^2(z,u)}. \tag{32}$$

In order to evaluate the integrals over z in Eqs. (30)–(32) at $\lambda<1$ (in the low-velocity limit) we split the integration region into two domains: $0\leqslant z\leqslant 1-u$ and $1-u\leqslant z\leqslant 1+u$, where Im $\varepsilon\sim f_2\neq 0$. However, at $\lambda>1$ (in high-velocity limit) we need to take into account the region $1\leqslant u\leqslant\lambda$, $0\leqslant z\leqslant u-1$, where f_2 may vanish. The integration in this region includes the excitation of collective plasma modes (plasmons) by fast charged particles. Consequently, although $f_2=0$, the integrals in this region are not equal to zero. A calculation of the collective part of SP is facilitated if we use the following known expression:

$$\frac{\chi^2f_2(z,u)}{[z^2+\chi^2f_1(z,u)]^2+\chi^4f_2^2(z,u)}\to\pi\delta[z^2+\chi^2f_1(z,u)] =\pi\frac{\delta[z-z_r(\chi,u)]}{|2z+\chi^2\partial f_1(z,u)/\partial z|_{z=z_r(\chi,u)}}, \tag{33}$$

where $z_r(\chi,u)$ is the solution of the dispersion equation $\varepsilon(k,\omega)=0$ in variables z and u.

Figure 19 shows the solution $z_r(\chi,u)$ for various values of χ (solid line, $\chi=0.5$; dashed line, $\chi=0.15$; dotted line, $\chi=0.05$). It may be noted that the integration domain $0\leqslant u\leqslant\lambda$, $z>u+1$, where $f_2=0$, does not contain the dispersion curve $z_r(\chi,u)$ calculated for metallic densities $\chi\sim0.5$ ($r_s\sim2$). Consequently the SP in this region of variables z and u vanishes and there is no plasmon excitation.

Let us consider the low-velocity limit ($V\ll v_F$) of Eqs. (30) and (31). In this limit one can obtain simpler expressions for SP. From Eqs. (30) and (31) we have

$$S_{\rm ind}(\lambda)\simeq\frac{\Sigma_0}{\pi\chi^2}\lambda\int_0^1\frac{z^3dz}{[z^2+\chi^2f(z)]^2}, \tag{34}$$

$$S_{\rm corr}(\lambda,R,\vartheta)\simeq\frac{3\Sigma_0}{2\pi\chi^2}\lambda\int_0^1\frac{z^3dz}{[z^2+\chi^2f(z)]^2}[\Phi_1(zk_FR) +\Phi_2(zk_FR)\sin^2\vartheta], \tag{35}$$

where

$$\Phi_1(\xi)=\frac{1}{\xi^3}\left[\left(\xi^2-\frac{1}{2}\right)\sin(2\xi)+\xi\cos(2\xi)\right], \tag{36}$$

$$\Phi_2(\xi)=\frac{1}{\xi^3}\left[\left(\frac{3}{4}-\xi^2\right)\sin(2\xi)-\frac{3}{2}\xi\cos(2\xi)\right], \tag{37}$$

$$f(z)\equiv f_1(z,0)=\frac{1}{2}+\frac{1-z^2}{4z}\ln\frac{1+z}{1-z}. \tag{38}$$

From Eqs. (36) and (37) it follows that $\Phi_1(\xi)\to2/3$, $\Phi_2(\xi)\to0$ at $\xi\to0$, and consequently, as expected, $S_{\rm corr}(\lambda,R,\vartheta)\to S_{\rm ind}(\lambda)$ when $R\to0$. Note that (as is well-known [4,13]) in the low-velocity limit the SP is proportional to the velocity of the particle [Eqs. (34) and (35)]. Thus the vicinage function $\Gamma(\lambda,R,\vartheta)$ at $\lambda\ll1$ depends only on interionic distance R and orientation angle ϑ.

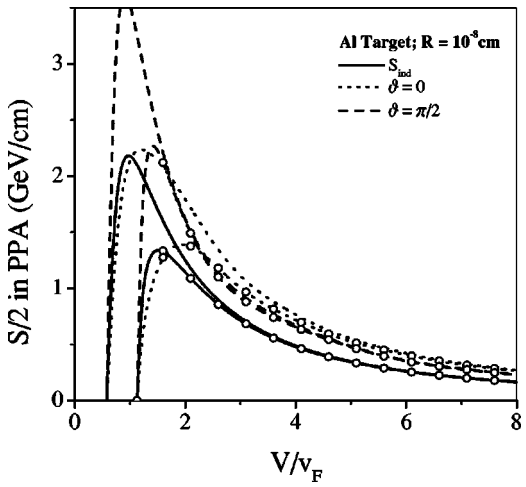

FIG. 1. $S/2$ of a diproton cluster with $R=10^{-8}$ cm, vs V/v_F for the Al target ($r_s=2.07$). $\vartheta=0$ (dotted line), $\vartheta=\pi/2$ (dashed line), and ISP (solid line). The lines with and without circles correspond to PPA with and without dispersion, respectively.

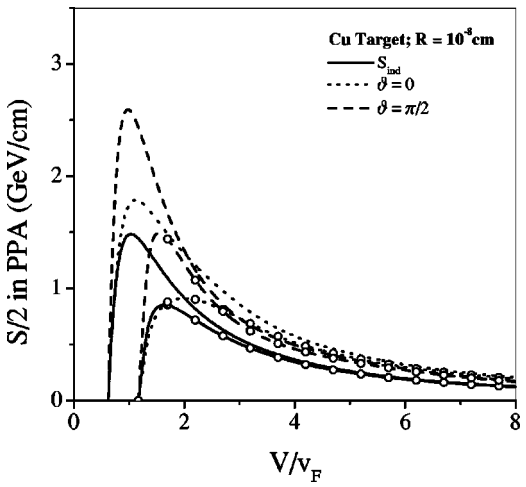

FIG. 3. $S/2$ of a diproton cluster with $R=10^{-8}$ cm, vs V/v_F for the Cu target ($r_s=2.68$). $\vartheta=0$ (dotted line), $\vartheta=\pi/2$ (dashed line), and ISP (solid line). The lines with and without circles correspond to PPA with and without dispersion, respectively.

IV. NUMERICAL RESULTS AND DISCUSSION

Using the theoretical results of Secs. II and III, we have made extensive numerical calculations of SP and related quantities. In this section we present detailed numerical results for two target materials, Al and Cu. These two targets have been chosen because of their frequent use in experiments and also because of their different electron densities. In our calculations χ (or r_s) is a measure of electron density.

As a simple but generic example of a projectile, we have considered a diproton cluster ($Z_1=Z_2=1$) for which we present theoretical results for the following quantities of physical interest: stopping power ($S/2$), vicinage function (Γ), angle-averaged stopping power ($S_{\rm av}/2=S_{\rm ind}+\overline{S}_{\rm corr}$), angle-averaged vicinage function ($\Gamma_{\rm av}=\overline{S}_{\rm corr}/S_{\rm ind}$) together with the dependence of $S/2$ and Γ on R, the interionic separation distance within the cluster. The reason why SP has been divided by a factor of 2 is that the SP results for a diproton cluster are expected to reduce asymptotically (as R tends to infinity) to those for two uncorrelated protons, the latter being referred to as individual SP (ISP). Angle-averaged SP (ASP) has been treated in the same way. We would like to mention that in the text we have used the notations e.g., SP, ISP, and ASP, and in the figures for the same quantities we have used S, $S_{\rm ind}$, and $S_{\rm av}$.

In our calculations of these quantities we have employed the linear-response approach, which assumes a swift ion-cluster projectile and also that the ion cluster presents a weak perturbation on the target plasma. The validity of the linear-response approach to study ion-cluster stopping has been discussed in detail by Zwicknagel and Deutsch [17]. We refer the reader to their insightful discussion.

We model the Al and Cu targets by a dense (degenerate) electron gas neutralized by a positive background (the jellium model) with electron densities appropriate for the respective targets [18]. The linear response of the target elec-

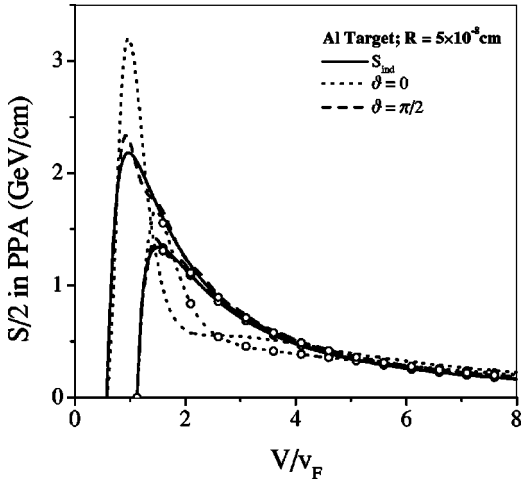

FIG. 2. $S/2$ of a diproton cluster with $R=5\times10^{-8}$ cm, vs V/v_F for the Al target. $\vartheta=0$ (dotted line), $\vartheta=\pi/2$ (dashed line), and ISP (solid line). The lines with and without circles correspond to PPA with and without dispersion, respectively.

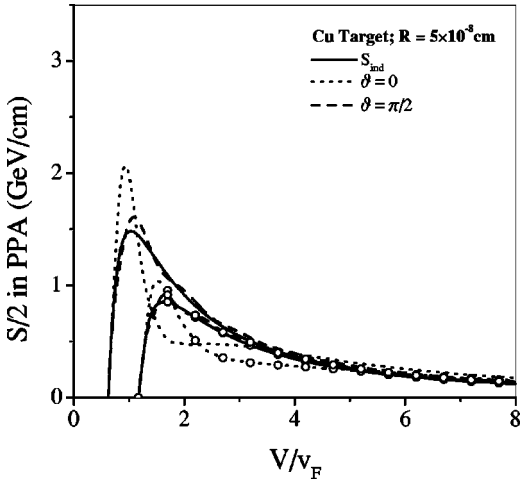

FIG. 4. $S/2$ of a diproton cluster with $R=5\times10^{-8}$ cm, vs V/v_F for the Cu target. $\vartheta=0$ (dotted line), $\vartheta=\pi/2$ (dashed line), and ISP (solid line). The lines with and without circles correspond to PPA with and without dispersion, respectively.

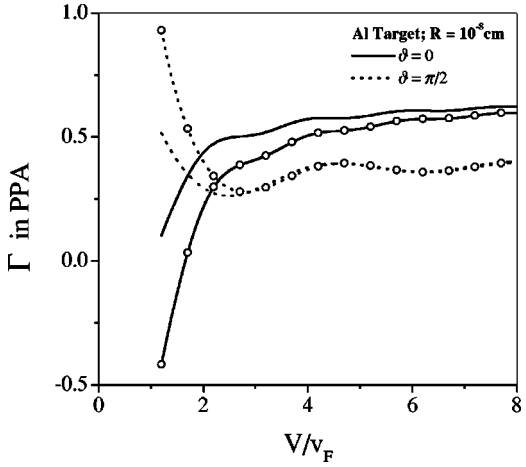

FIG. 5. VF of a diproton cluster with $R=10^{-8}$ cm, vs V/v_F for the Al target. $\vartheta=0$ (solid line) and $\vartheta=\pi/2$ (dotted line). The lines with and without circles correspond to PPA with and without dispersion, respectively.

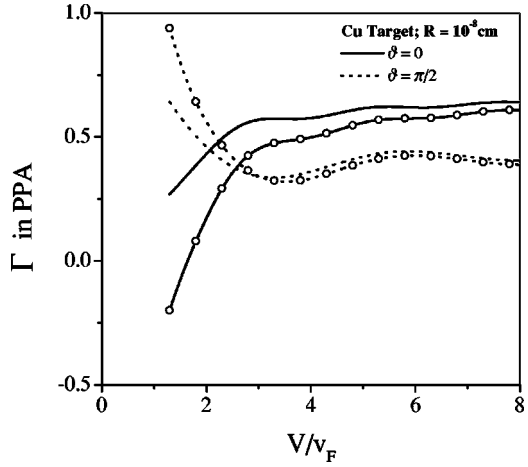

FIG. 7. VF of a diproton cluster with $R=10^{-8}$ cm, vs V/v_F for the Cu target. $\vartheta=0$ (solid line) and $\vartheta=\pi/2$ (dotted line). The lines with and without circles correspond to PPA with and without dispersion, respectively.

tron gas, which couples the cluster projectile to the target, is considered at three levels of approximations to the dielectric function $\varepsilon(k,\omega)$ as discussed in Secs. II and III. In the context of stopping power these approximations are subject to the following general remarks: The PPA is valid only in the high-velocity regime when the mean velocity V of the cluster is $>v_F$, the Fermi velocity of the target electrons. For $V<v_F$ and for velocities near the threshold of collective mode excitations, this approximation is not adequate. The RPA overcomes this limitation although it cannot account for short-range correlations in the electron gas. Within PPA itself, PPA-1 (without plasmon dispersion) is more limited than PPA-2 (with plasmon dispersion). The figures we present serve as a comparative study of how these levels of approximation affect the various physical quantities related to stopping power.

Figures 1–4 show cluster stopping power (SP and its dependence on various quantities of experimental interest). Let us first note that these figures are presented for two specific values, 0 and $\pi/2$, of the angle ϑ. Correlations between the two ions in the dicluster are maximum and minimum, respectively, for these two values of ϑ. The objective is then to see how, for these maximum and minimum configurations, SP depends on R and V/v_F. Figure 1 shows SP for Al target with $R=10^{-8}$ cm, as a function of V/v_F for the two above-mentioned values of ϑ, within PPA. The lines without circles correspond to PPA-1 and, with circles, to PPA-2. The angular dependence of SP is particularly noteworthy. It is seen that in a medium velocity range ($V<2v_F$), SP has a remarkably higher value for the larger value of ϑ. This is likely due to single-particle excitations in this velocity range. In the higher velocity range, the dicluster wake-field excitations become important and we find that the situation is reversed in the higher velocity range ($V>2v_F$) for which SP for $\vartheta=0$ is larger than for $\vartheta=\pi/2$.

In the low-velocity range the difference between PPA-1 and PPA-2 (for both $\vartheta=0$ and $\pi/2$) is noticeable while in the high-velocity range this difference becomes negligible. This is again due to single-particle excitations in the low-

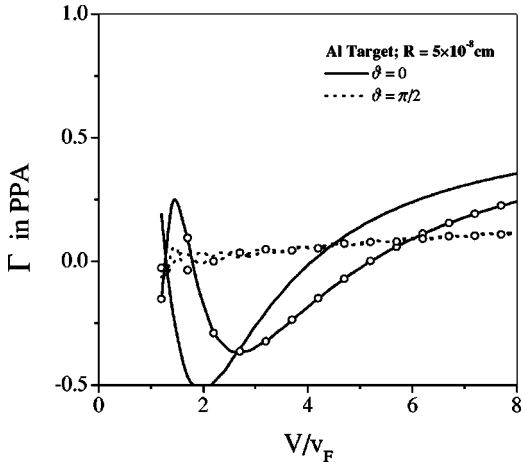

FIG. 6. VF of a diproton cluster with $R=5\times10^{-8}$ cm, vs V/v_F for the Al target. $\vartheta=0$ (solid line) and $\vartheta=\pi/2$ (dotted line). The lines with and without circles correspond to PPA with and without dispersion, respectively.

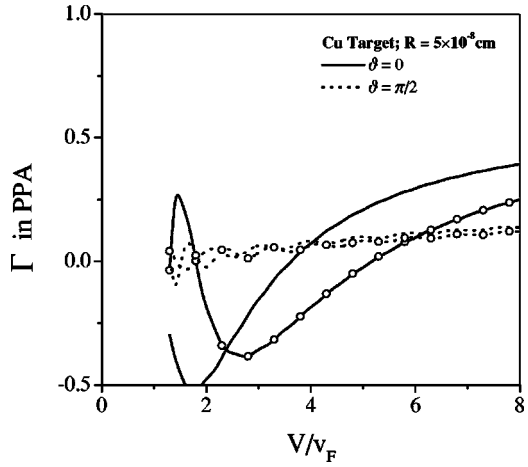

FIG. 8. VF of a diproton cluster with $R=5\times10^{-8}$ cm, vs V/v_F for the Cu target. $\vartheta=0$ (solid line) and $\vartheta=\pi/2$ (dotted line). The lines with and without circles correspond to PPA with and without dispersion, respectively.

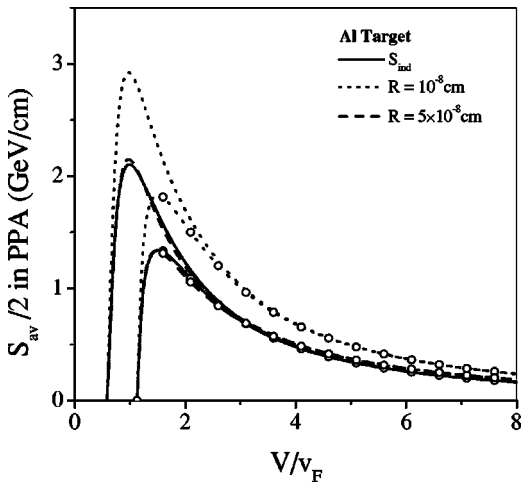

FIG. 9. $S_{\mathrm{av}}/2$ of a diproton cluster with $R=10^{-8}$ cm (dotted line) and $R=5\times10^{-8}$ cm (dashed line) vs V/v_F for the Al target. Solid line, ISP. The lines with and without circles correspond to PPA with and without dispersion, respectively.

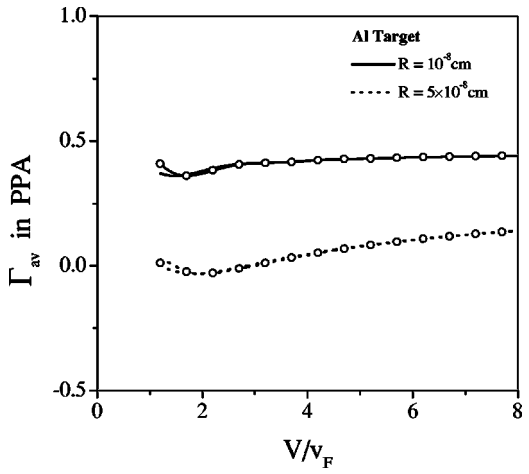

FIG. 11. AVF of a diproton cluster with $R=10^{-8}$ cm (solid line) and $R=5\times10^{-8}$ cm (dotted line) vs V/v_F for the Al target. The lines with and without circles correspond to PPA with and without dispersion, respectively.

velocity range. For comparison, we have also presented the uncorrelated stopping power (S_{ind}).

When we increase the interionic separation distance R from 10^{-8} cm to 5×10^{-8} cm, keeping other physical parameters the same, some interesting changes occur, as can be seen from Fig. 2. A noticeable change is that now, for $V<2v_F$, SP for $\vartheta=0$ is higher than that for $\vartheta=\pi/2$. This sensitivity of SP to the angle ϑ, as R is varied, may be due a combination of factors. The dicluster behaves like a compact project for small R, and like an extended projectile for large R. This has a bearing on S_{corr} given in Eqs. (13) and (22). Correlation effects are expected to be maximum when the two ions are aligned with each other in the direction of propagation of the dicluster projectile motion ($\vartheta=0$) while they decay (at least for $V>v_F$) when ϑ tends to $\pi/2$, the latter behavior being related to the wake-field due to the leading ion. The oscillation amplitude in S_{corr} tends to decrease from $\vartheta=0$ to $\vartheta=\pi/2$ (the Čherenkov cone). However when R is small, each ion is influenced by the unscreened field of the other ion. For model solid targets, the Čherenkov cone semivertex is $\vartheta_C=\arcsin(\sqrt{0.6}v_F/V)$ [18]. ϑ_C is approximately equal to 22.8°, 7.4°, and 0.08° for $V=2v_F$, $V=6v_F$, and $V=10v_F$, respectively. Consequently in the high-velocity range the trailing ion moves inside the Čherenkov cone of the leading ion only for almost aligned diclusters. The behavior of SP shown in Figs. 1 and 2 reflects these features within the linear response and for PPA. It will be noted that the high values of SP are due to the PPA-1 approximation. PPA-2 decreases these values to a small extent. Later, when we use a more realistic, namely, RPA, for the linear-response function (Figs. 20–23) SP considerably decreases in strength.

Figures 3 and 4 show SP for Cu, another commonly used metallic target. These figures show patterns similar to those in Figs. 1 and 2, except that SP and ISP have lower values over the entire range of V/v_F. This is because Al has a higher-electron density than Cu.

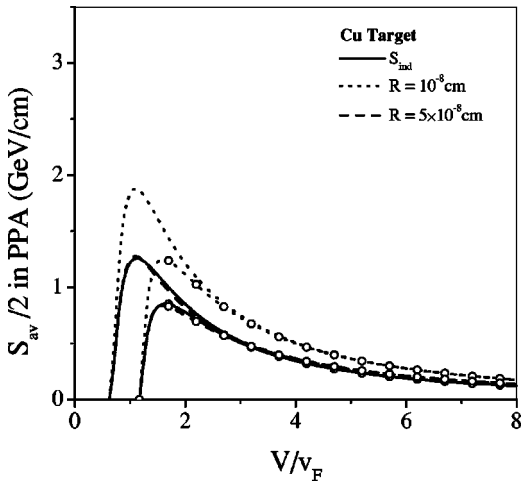

FIG. 10. $S_{\mathrm{av}}/2$ of a diproton cluster with $R=10^{-8}$ cm (dotted line) and $R=5\times10^{-8}$ cm (dashed line) vs V/v_F for the Cu target. Solid line, ISP. The lines with and without circles correspond to PPA with and without dispersion, respectively.

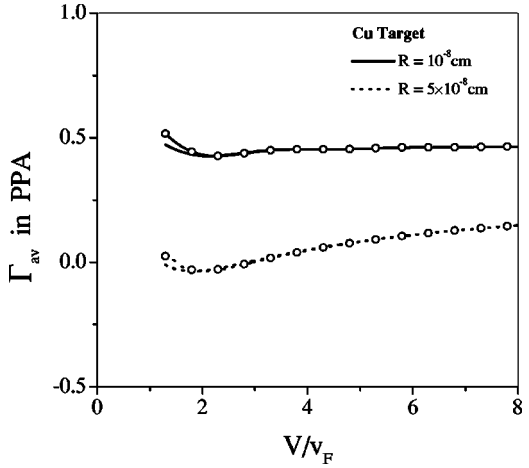

FIG. 12. AVF of a diproton cluster with $R=10^{-8}$ cm (solid line) and $R=5\times10^{-8}$ cm (dotted line) vs V/v_F for the Cu target. The lines with and without circles correspond to PPA with and without dispersion, respectively.

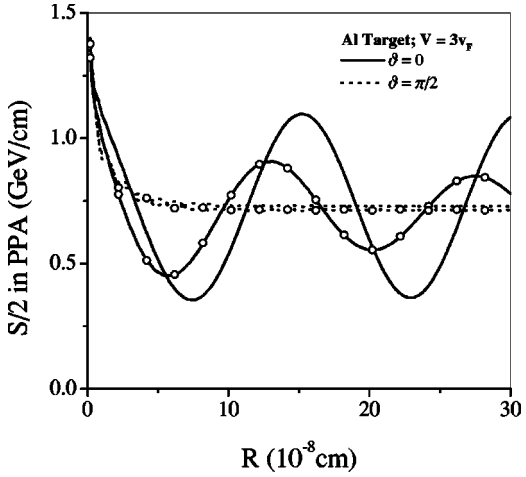

FIG. 13. $S/2$ of a diproton cluster with $V=3v_F$ vs R for the Al target. $\vartheta=0$ (solid line), $\vartheta=\pi/2$ (dotted line). The lines with and without circles correspond to PPA with and without dispersion, respectively.

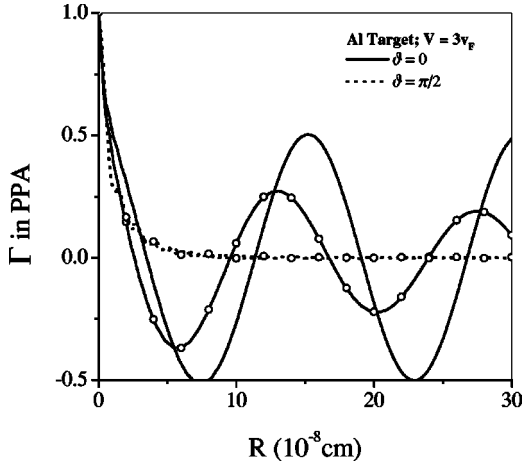

FIG. 15. VF of a diproton cluster with $V=3v_F$ vs R for the Al target. $\vartheta=0$ (solid line) and $\vartheta=\pi/2$ (dotted line). The lines with and without circles correspond to PPA with and without dispersion, respectively.

The vicinage function (VF) given by Eq. (8) has been plotted as a function of the beam velocity for Al target in Figs. 5 and 6. This function shows an interplay between ϑ and R more strikingly than SP. Figures 7 and 8 display a similar behavior for Cu target.

As stated in Sec. II, an ASP is of experimental interest. Figures 9 and 10 show ASP for Al and Cu, respectively. ISP is also shown, for comparison. The role of PPA-1 and PPA-2 is now more clearly seen.

In the same spirit we have plotted averaged vicinage function (AVF) for Al and Cu in Figs. 11 and 12. The role of R is highlighted in these figures. However it will be noticed that PPA-1 and PPA-2 make practically no distinction for AVF.

We have so far plotted SP or ASP (divided by a factor of 2 in both the cases) vs the beam velocity V/v_F, for some values of the separation distance R. We now look for some complementary information about SP, and plot SP as a function of R with $V=3v_F$, for an Al target. Figure 13 shows an oscillatory character of SP with respect to R. The oscillations are the highest for $\vartheta=0$ and lowest for $\vartheta=\pi/2$. The role of PPA-1 and PPA-2 is clearly seen for $\vartheta=0$. Figure 14 shows a similar behavior of SP for Cu although the amplitudes are now weaker. In the same way VF is plotted in Figs. 15 and 16, for Al and Cu targets, respectively.

Figure 17 shows ASP vs R for both Al and Cu targets. The difference between PPA-1 and PPA-2 is negligible and the Cu target has ASP smaller than for Al. Now, there is something interesting about Fig. 18 that shows AVF. The difference between PPA-1 and PPA-2 is again negligible. But let us note that data for both Al and Cu lie practically on the same curve! Recalling the definition of VF, Eq. (8), one can see from Eqs. (12), (16), (21), and (26) that AVF has a weak dependence on target density. Also, when $\lambda=V/v_F>2$, S_{ind} does not noticeably depend on PPA-1 and PPA-2. These features combine to lead to the behavior of AVF as seen in Fig. 18.

We have so far presented results for PPA-1 and PPA-2. A more realistic linear-response function, namely, the exact

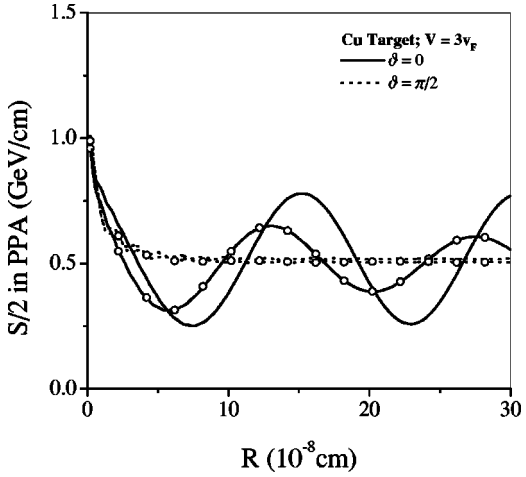

FIG. 14. $S/2$ of a diproton cluster with $V=3v_F$ vs R for the Cu target. $\vartheta=0$ (solid line) and $\vartheta=\pi/2$ (dotted line). The lines with and without circles correspond to PPA with and without dispersion, respectively.

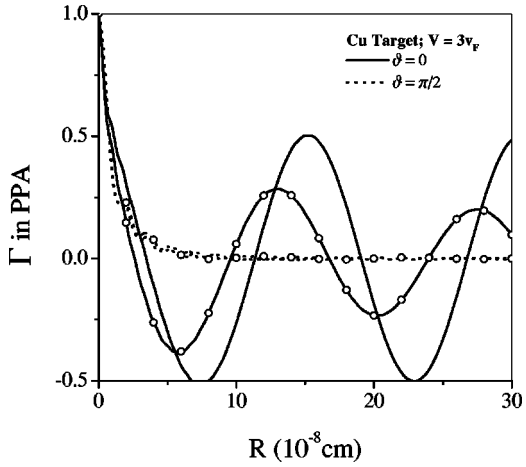

FIG. 16. VF of a diproton cluster with $V=3v_F$ vs R for the Cu target. $\vartheta=0$ (solid line) and $\vartheta=\pi/2$ (dotted line). The lines with and without circles correspond to PPA with and without dispersion, respectively.

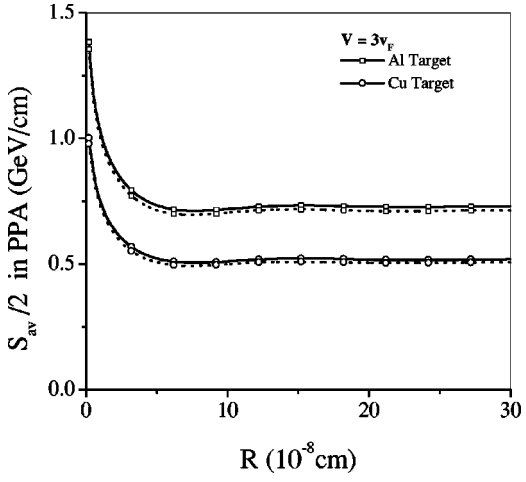

FIG. 17. $S_{\mathrm{av}}/2$ of a diproton cluster with $V=3v_F$ vs R for the Al (the lines with square symbols) and Cu (the lines with circles) targets. Dotted and solid lines, PPA with and without dispersion, respectively.

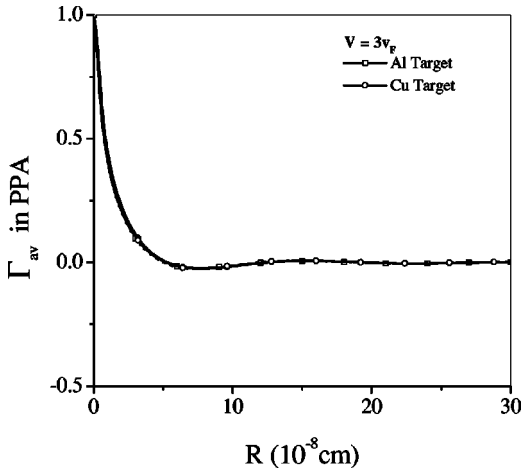

FIG. 18. AVF of a diproton cluster with $V=3v_F$ vs R for the Al (the lines with square symbols) and Cu (the lines with circles) targets. Dotted and solid lines, PPA with and without dispersion, respectively.

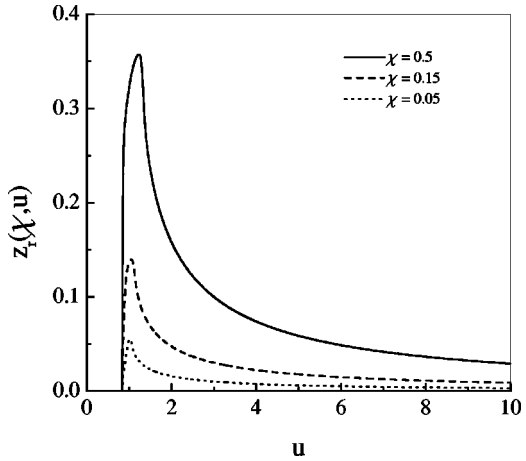

FIG. 19. Relation between $z_r(\chi,u)$ and u, as obtained from the dispersion equation $\varepsilon(z_r,u)=0$. $\chi=0.5$ (solid line); $\chi=0.15$; (dashed line) $\chi=0.05$ (dotted line).

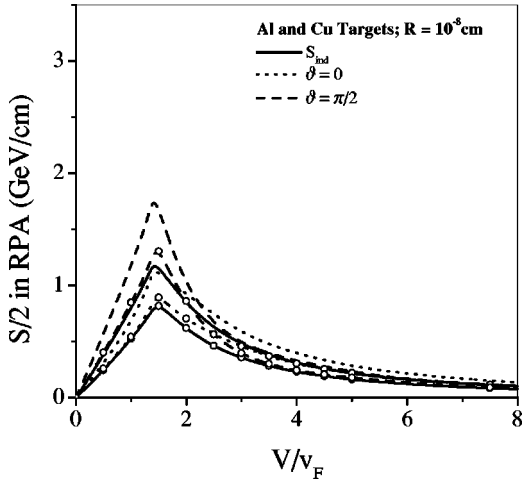

FIG. 20. $S/2$ of a diproton cluster with $R=10^{-8}$ cm in a RPA vs V/v_F for the Al (the lines without symbols) and Cu (the lines with circles) targets. $\vartheta=0$ (dotted line), $\vartheta=\pi/2$ (dashed line), and ISP (solid line).

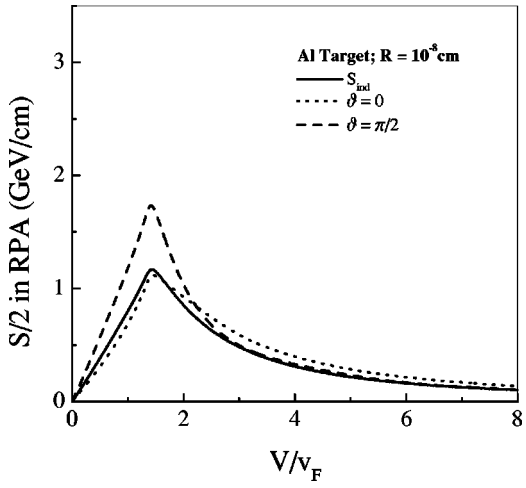

FIG. 21. $S/2$ of a diproton cluster with $R=10^{-8}$ cm in a RPA vs V/v_F for the Al target. $\vartheta=0$ (dotted line), $\vartheta=\pi/2$ (dashed line), and ISP (solid line).

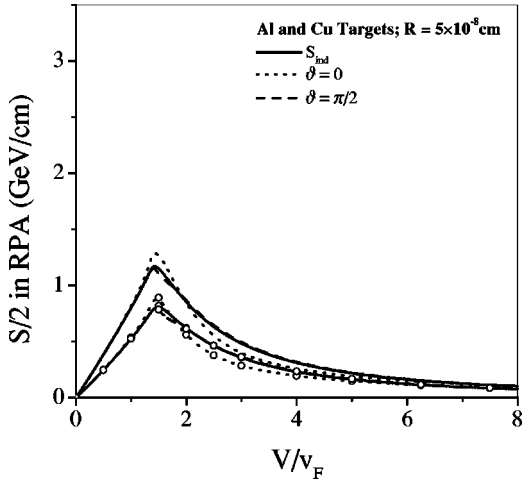

FIG. 22. $S/2$ of a diproton cluster with $R=5\times10^{-8}$ cm in a RPA vs V/v_F for the Al (the lines without symbols) and Cu (the lines with circles) targets. $\vartheta=0$ (dotted line), $\vartheta=\pi/2$ (dashed line), and ISP (solid line).

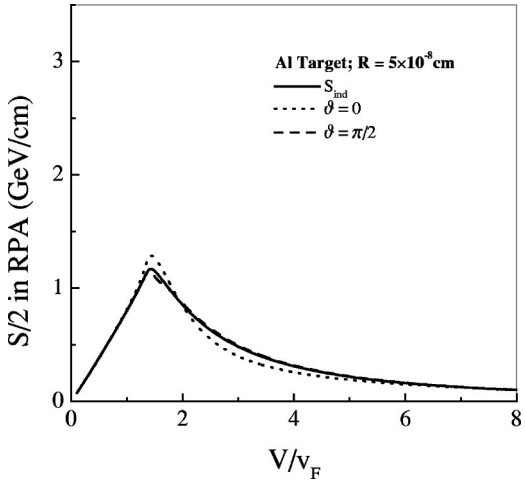

FIG. 23. $S/2$ of a diproton cluster with $R=5\times10^{-8}$ cm in a RPA vs V/v_F for the Al target. $\vartheta=0$ (dotted line), $\vartheta=\pi/2$ (dashed line), and ISP (solid line).

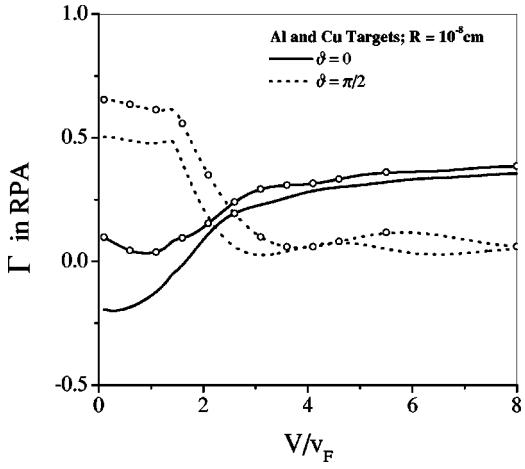

FIG. 24. VF of a diproton cluster with $R=10^{-8}$ cm in a RPA vs V/v_F for the Al (the lines without symbols) and Cu (the lines with circles) targets. $\vartheta=0$ (solid line) and $\vartheta=\pi/2$ (dotted line).

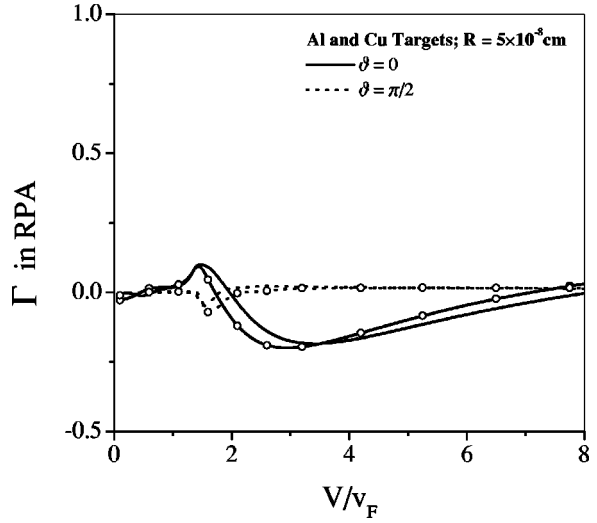

FIG. 25. VF of a diproton cluster with $R=5\times10^{-8}$ cm in a RPA vs V/v_F for the Al (the lines without symbols) and Cu (the lines with circles) targets. $\vartheta=0$ (solid line) and $\vartheta=\pi/2$ (dotted line).

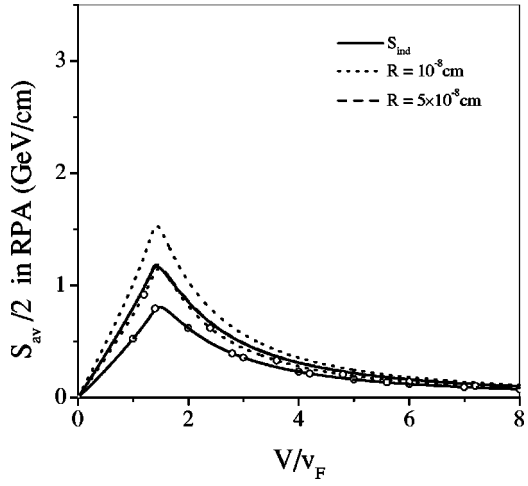

FIG. 26. $S_{\rm av}/2$ of a diproton cluster with $R=10^{-8}$ cm (dotted line) and $R=5\times10^{-8}$ cm (dashed line) in a RPA vs V/v_F for the Al (the lines without symbols) and Cu (the lines with circles) targets and ISP (solid line).

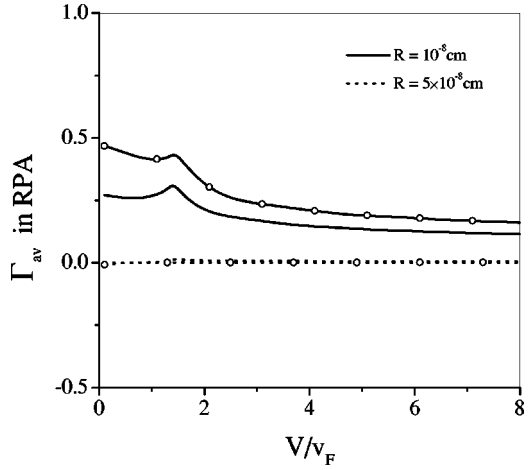

FIG. 27. AVF of a diproton cluster with $R=10^{-8}$ cm (solid line) and $R=5\times10^{-8}$ cm (dotted line) in a RPA vs V/v_F for the Al (the lines without symbols) and Cu (the lines with circles) targets.

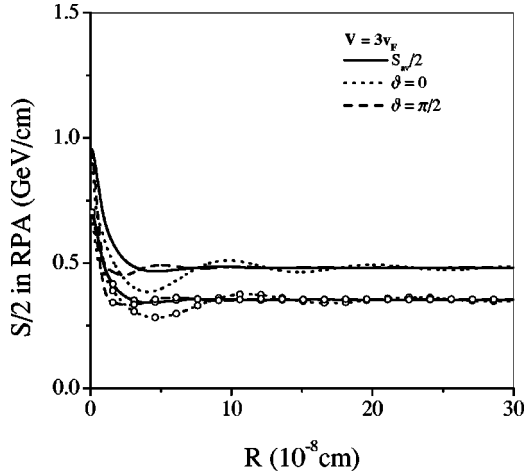

FIG. 28. $S/2$ of a diproton cluster with $V=3v_F$ in a RPA vs R for the Al (the lines without symbols) and Cu (the lines with circles) targets; $S_{\rm av}/2$ (solid line), $\vartheta=0$ (dotted line), and $\vartheta=\pi/2$ (dashed line).

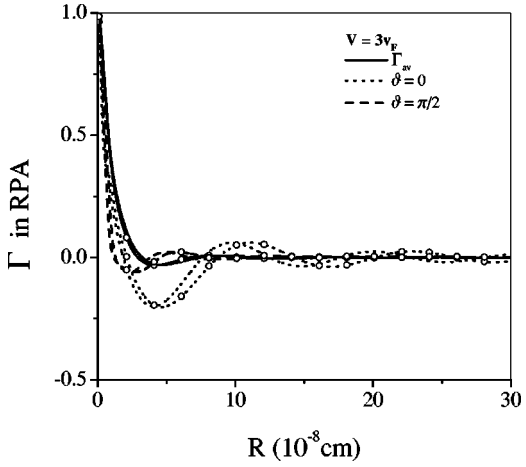

FIG. 29. VF of a diproton cluster with $V=3v_F$ in a RPA vs R for the Al (the lines without symbols) and Cu (the lines with circles) targets, AVF (solid line), $\vartheta=0$ (dotted line), and $\vartheta=\pi/2$ (dashed line).

RPA will now be used for the metallic target. The theoretical results for SP, etc., have been presented in Sec. III C. As part of calculating SP in RPA, it is useful to examine the plasmon dispersion obtained through $\varepsilon(z_r,u)=0$, where z and u have been defined in Sec. III C. Figure 19 displays $z_r(\chi,u)$ vs u for three electron-density parameter values.

Next we present ISP and SP in RPA, for Al and Cu in Figs. 20 and 22, corresponding to $R=10^{-8}$cm and $R=5\times10^{-8}$cm, respectively. For the sake of a better presentation of the data we have also separately displayed the Al data in Figs. 21 and 23. The RPA results show that SP and ISP decrease in strength with an improved linear-response function. This should be of relevance to experiments.

Next, VF in RPA vs V/v_F is presented in Fig. 24, for Al (lines without circles) and for Cu (lines with circles), corresponding to $R=10^{-8}$ cm and for $\vartheta=0$ and $\pi/2$. This figure may be compared with Figs. 5 and 7. For $V/v_F<2$, the curves for VF in RPA tend toward finite values whereas the VF curves in PPA do not, although the angular trend is similar. A similar contrast may be noted between Figs. 6 and 8, and Fig. 25, corresponding to $R=5\times10^{-8}$ cm. Again, these findings are of experimental relevance.

Averaged SP vs V/v_F in RPA is presented in Fig. 26, for Al (curves without circles) and for Cu (curves with circles) along with ISP, corresponding to $R=10^{-8}$ cm and 5×10^{-8} cm. This figure may be compared with Figs. 9 and 10. Figure 26 shows an expected overall decrease in the strength of ASP in RPA.

There are similarities but also some interesting differences if we compare Figs. 11 and 12 with Fig. 27. The latter shows AVF in RPA for Al (curves without circles) and for Cu (curves with circles). The differences are more noteworthy for $R=10^{-8}$ cm.

SP vs R in RPA is plotted in Fig. 28, corresponding to $V=3v_F$, for Al and Cu in the previously stated scheme. When Fig. 28 is compared with Figs. 13 and 14, the differences between PPA and RPA become particularly striking.

A similar contrast is provided by a comparison of Fig. 29 with Figs. 15 and 16, for VF vs R in RPA and PPA, corresponding to $V=3v_F$ and for $\vartheta=0$ and $\pi/2$. For comparison AVF is also plotted in Fig. 29.

This completes our extensive presentation of figures exhibiting various aspects of the stopping power of a diproton cluster in PPA and RPA, for Al and Cu targets.

V. SUMMARY

In this paper we have presented a comprehensive theoretical study of stopping power of a dicluster of protons in a metallic target. After a general introduction to SP of a cluster of two pointlike ions, in Sec. II, theoretical calculations of SP based on the linear-response theory and using PPA without and with plasmon dispersion and then with RPA, are discussed in Sec. III. The theoretical expressions for a number of physical quantities derived in Sec. III lead to a detailed presentation, in Sec. IV, of a large collection of data through figures on correlated stopping power, vicinage function, average stopping power, and average vicinage function of a diproton cluster projectile for two metallic targets, Al and Cu. Whenever relevant, we have also provided a plot of independent (i.e., single-ion) stopping power for comparison.

With the proviso stated in Sec. IV, SP and related quantities have been studied within a linear-response formalism; some analytical and all numerical results have been obtained corresponding to three approximations to the dielectric function of the target electron gas—the PPA without dispersion (PPA-1) and with dispersion (PPA-2), and also with the RPA. To our knowledge this is the most comprehensive calculation of the SP-related physical quantities using all the three dominant approximations to the linear-response function. The results we have presented demonstrate that with regard to several physical quantities of primary interest the difference between PPA and RPA is substantial while for others, especially for average quantities, this difference may not be of practical significance.

It will be of interest to go beyond RPA in order to include some short-range correlations in the electron gas and to study how dicluster SP is affected. However calculating the linear-response function by including electron energy bands is rather involved and detailed theoretical studies of SP with band-structure effects included have not yet been reported in the literature. One can include some aspect of band structure in a rather approximate manner through an effective mass for the electrons.

Another aspect we have not considered in this paper is some effect of disorder in the target medium. In real metals electrons suffer collisions with impurities, etc. We intend to address this issue in the context of stopping power in a separate study.

ACKNOWLEDGMENTS

It is a pleasure to thank to Dr. G. Zwicknagel for useful discussions. The authors are grateful to V. Nikoghosyan for technical assistance.

[1] P. M. Echenique, F. Flores, and R. H. Ritchie, Solid State Phys. **43**, 229 (1990).
[2] J. F. Ziegler, J. Appl. Phys. **85**, 1249 (1999).
[3] D. Bohm and D. Pines, Phys. Rev. **82**, 625 (1951); , **85**, 338 (1952).
[4] J. Lindhard, Mat. Fys. Medd. K. Dan. Vidensk. Selsk. **28**, 1 (1954); J. Lindhard and A. Winther, *ibid.* **34**, 1 (1964).
[5] R. H. Ritchie, Phys. Rev. **114**, 644 (1959).
[6] Yu. N. Yavlinsky, Zh. Éksp. Teor. Fis. **80**, 1622 (1981) [Sov. Phys. JETP **53**, 835 (1981)].
[7] D. G. Yakovlev and S. S. Kotel'nikov, Zh. Éksp. Teor. Fis. **84**, 1348 (1983) [Sov. Phys. JETP **57**, 781 (1983)].
[8] R. H. Ritchie, C. J. Tung, V. E. Anderson, and J. C. Ashley, Radiat. Res. **64**, 181 (1975); T. L. Ferrell and R. H. Ritchie, Phys. Rev. B **16**, 115 (1977); C. J. Tung and R. H. Ritchie, *ibid.* **16**, 4302 (1977).
[9] N. R. Arista, Phys. Rev. B **18**, 1 (1978).
[10] G. Basbas and R. H. Ritchie, Phys. Rev. A **25**, 1943 (1982).
[11] P. M. Echenique, Nucl. Instrum. Methods Phys. Res. B **27**, 256 (1987).
[12] N. R. Arista and W. Brandt, Phys. Rev. A **23**, 1898 (1981); T. A. Mehlhorn, J. Appl. Phys. **52**, 6522 (1981); N. R. Arista and A. R. Piriz, Phys. Rev. A **35**, 3450 (1987).
[13] G. Maynard and C. Deutsch, Phys. Rev. A **26**, 665 (1982).
[14] J. D' Avanzo, M. Lontano, and P. F. Bortignon, Phys. Rev. E **47**, 3574 (1993).
[15] C. Deutsch, Phys. Rev. E **51**, 619 (1995).
[16] C. Deutsch, Laser Part. Beams **8**, 541 (1990).
[17] G. Zwicknagel and C. Deutsch, Phys. Rev. E **56**, 970 (1997).
[18] W. Schäfer, H. Stöcker, B. Müller, and W. Greiner, Z. Phys. A **8**, 349 (1978).